Investigation of Case II Diffusion Behavior. 2. Study of the Poly(methyl methacrylate)−Methyl Alcohol System by Two-Beam Microinterferometry

D. F. Stamatialis,† M. Sanopoulou,* and J. H. Petropoulos

Physical Chemistry Institute, Demokritos National Research Center, GR-15310 Aghia Paraskevi, Athens, Greece

Received August 9, 2000; Revised Manuscript Received June 18, 2001

ABSTRACT: Results are reported of an experimental investigation of penetration rate and penetrant concentration profile, in the PMMA−methyl alcohol (MA) system. Penetration of liquid MA, at 22, 30, and 40 °C, *along* annealed or quenched films sandwiched between glass plates, was followed microscopically, and the corresponding concentration profile was studied by two-beam microinterferometry. This experimental approach was shown to provide information not directly obtainable by sectioning followed by colored tracer microdensitometry or by laser interferometry, previously applied to the study of MA *across* the PMMA film. On the basis of this new experimental evidence, in conjunction with the results of the theoretical investigation reported in part 1, it proved possible to elucidate certain important, but previously obscure, aspects of case II diffusion behavior in this system.

Introduction

In the preceding paper,[1] reference was made to certain outstanding questions bearing on the present state of our knowledge with regard to certain important aspects of case II liquid diffusion into polymer films. An account was then given of a detailed theoretical model investigation, which yielded some significant new insights into the role of certain salient polymer−penetrant parameters in the determination of both penetration rate and concentration profile shape.

Here, we report the results of an experimental investigation of penetration rates and concentration profiles in the poly(methyl methacrylate) (PMMA)−methyl alcohol (MA) system. Detailed data of case II penetration rate behavior, with parallel theoretical model interpretation thereof, have been given for this system by Thomas and Windle (TW).[2,3] Nevertheless, for the reasons indicated in part 1, the reported optical density profiles of iodine, which was used as a colored tracer, cannot be taken as reasonably faithful representations of MA concentration profiles in all respects, without prior careful validation.

The interferometric technique applied by Durning et al. (CD)[4,5] may certainly be considered more reliable. An important experimental variable measured thereby is the reflectivity of the penetration front, which is very sensitive to its overall steepness. However, the interpretation of the relevant interference pattern is model-dependent. CD[4,5] used for this purpose the simple "step-cum-exponential precursor front" model of Hui et al.[6,7] On this basis, it proved impossible to comprehend certain salient aspects of the observed behavior. Thus, the increase of penetration velocity with temperature was paralleled (as expected) by the reflectivity, but only up to a certain point, beyond which the reflectivity began to decline. On the other hand, the increase in penetration velocity induced by various types of quenching treatment was accompanied by a decline (rather than the theoretically expected rise) in reflectivity.

The advantage of the microinterferometric method used by us[8,9] is that it yields a refractive index profile, which is *directly* related to that of penetrant concentration. Here the film is pressed between glass plates to ensure penetration along the plane of the film (and at right angles to the incident light beam). This imposes an external constraint, which may affect materially the mode and extent of swelling (and hence the concentration profile) of the penetrated portion of the film. (Note that, in the techniques employed by TW and CD, penetration occurs across the film; in the former case, there is symmetrical two-sided penetration into an externally unconstrained film whereas, in the latter case, one-sided penetration occurs into a very thin supported film.)

It is thus clear that each of the aforementioned techniques has its own specific capabilities and peculiarities; hence, their application to the same polymer−penetrant system appeared promising. Indeed, as shown below, the data furnished by the present work helped materially to fill the gaps left by those of TW and CD. At the same time, the fuller phenomenological picture which thus emerged turned out to be fully self-consistent and comprehensible, in the light of relevant theoretical results reported in part 1.

The notation of part 1 is maintained here, except that ℓ (which delimits the half-space along the axis of penetration used in the model calculations of part 1) is here replaced by X_{AB}, the distance of the sharp penetrant front from the edge of the swollen film.

Experimental Section

Materials. PMMA powder was obtained from Aldrich (code number 18223-0). The following specifications were given by the manufacturer: average M_n = 67K; M_w = 134K; T_g = l14 °C. MA was of analytical reagent grade.

Polymer films of thickness L = 30−40 μm were prepared by casting a 20% by weight solution of the polymer powder in acetone on a glass surface. After evaporation of the solvent in

* Corresponding author. Telephone: +30-1-6503785. Fax: +30-1-6511766. E-mail: sanopoul@mail.demokritos.gr.

† Present address: European Membrane Institute, Twente, University of Twente, Chemical Technology Department, P.O. Box 217, NL-7500 AE Enschede, The Netherlands.

10.1021/ma001409b CCC: $22.00 © 2002 American Chemical Society
Published on Web 01/03/2002

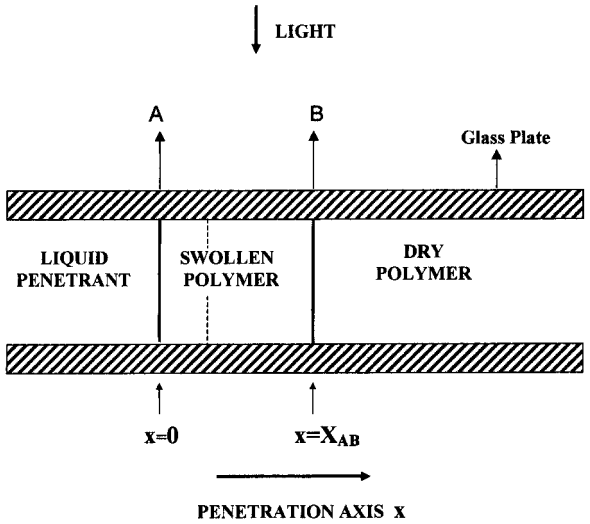

Figure 1. Schematic side view of the experimental setup.

the atmosphere, the film was removed from the glass plate, heated gradually in an oven, over a period of 24 h, to 130 °C, and maintained at that temperature for 24 h. Following this, "annealed" films were gradually cooled to 70 °C, maintained at that temperature for 24 h, and then allowed to cool slowly to room temperature; while "quenched" films were immersed in ice water or in liquid nitrogen for 2 min.

Measurement of Penetration Rate. Unidimensional penetration rate and kinetics along the plane of the film was measured as follows: a 3×5 mm^2 film sample was sandwiched between two glass plates held together by spring clips (Figure 1). The said glass plates had previously been smeared with extremely thin films of silicone grease, to minimize friction between film and glass plates and thus facilitate swelling of the polymer by back flow along the direction of penetration. (The thin grease films in question had no discernible effect on the interferometric fringe pattern described below.) The sandwiched film was immersed in a bath of liquid MA thermostated at the desired temperature and was periodically quickly transferred (along with a sufficient amount of liquid MA) in a Petri dish to the stage of a microscope (Amplival Pol-U of Jena, Germany). The edge of the swelling film (front A) and the penetrant front B (see Figure 1) mark relatively sharp changes in the gradient of concentration, and hence of the refractive index, and are seen in the microscope as dark lines.

The distance X_{AB} between these lines was recorded, and plotted as a function of time t. Note that the space coordinate along the penetration axis x is here defined in laboratory coordinates, using front A as origin.

Microinterferometry. The aforementioned microscope was also equipped with a two-beam Mach-Zehnder interferometer, which generates fringes aligned with the direction of penetration. The fringe pattern could be recorded using an attached CCD camera connected to a PC. The variation of refractive index along the x axis in the penetrated film is reflected in lateral fringe displacements, which are proportional to the corresponding optical path differences (OPD's). The fringe displacement at any location x within the penetrated film $\Delta y(x)$ varies during the course of the experiment and must, therefore, be measured relative to the location of the same fringe in the adjoining liquid, which remains fixed. Thus, the OPD profile, normalized with respect to the OPD of the unpenetrated film Δy_0, is given by

$$\frac{\Delta y(x)}{\Delta y_0} = \frac{n(x)L_x - n_1L_1}{n_2L_2 - n_1L_1} \tag{1}$$

In eq 1, n is the refractive index and L the film thickness. Subscripts 1 and 2 refer to the pure liquid MA and pure (unpenetrated) polymer respectively; $n(x)$ and L_x denote the refractive index and thickness of the swollen (penetrated) polymer at x.

As indicated by eq 1, under conditions of reasonably uniform film thickness (i.e. $L_x = L_1 = L_2$), the OPD profile represents faithfully the refractive index profile. Measurement of n as a function of penetrant concentration C then yields the required concentration profile. However, reasonable conformity to a linear relation between penetrant concentration C and refractive index is commonly observed over a wide concentration range, leading to

$$\bar{V}_1C(x) = 1 - \frac{n(x) - n_1}{n_2 - n_1} \tag{2}$$

where $\bar{V}_1$ is the molar volume of pure penetrant. In the case of uniform thickness, eq 2 reduces to

$$\bar{V}_1C(x) = 1 - \frac{\Delta y(x)}{\Delta y_0} \tag{2a}$$

thus providing a direct link between concentration and measured OPD profile.

Microdensitometry. As in ref 2, iodine was used as a colored tracer. Accordingly, the sandwiched polymer film was immersed in MA containing 40 g dm^{-3} of iodine. At the appropriate time, the sandwiched film was removed from the bath; the MA present in the gaps between the glass plates surrounding the film specimen was quickly sealed in with glue; and the film specimen was scanned along the direction of penetration on the stage of a microdensitometer (Joyce and Loebl, type 3CS). The optical density profile was recorded at a chart-to-stage ratio of 1000:1.

Results

The behavior of "annealed" and "quenched" films (prepared as indicated in the experimental section) was investigated at three different temperatures (22, 30, and 40 °C) and compared with that observed by CD.

Penetration Rates. Representative data are displayed in Figure 2, and the corresponding penetration rate Arrhenius plots are shown in Figure 3. A comparison with the absorption rate into free annealed films (corresponding to the experimental conditions of ref 2) was made at 22 °C. For this purpose $40 \times 40 \times 0.09$ mm^3 film samples were immersed in liquid MA and periodically withdrawn, blotted, and weighed. An example of the results is shown in Figure 4. The fact that good agreement was found between the rate of weight gain of free films and the penetration rate into sandwiched films indicates (i) absence of significant film anisotropy and (ii) absence of material effect of clamping on penetration rate. It is also noteworthy that the Arrhenius activation energy of the penetration velocity E_v^a into annealed films deduced from Figure 2 amounts to 23.7 ± 0.3 kcal/mol; this is in good agreement with $E_v^a = 24.5 \pm 1.1$ kcal/mol reported by CD for penetration across supported spin-cast and annealed films (while a typical penetration rate of 1 μm/min at 30 °C in ref 4 compares very favorably with the corresponding mean value of 0.8 μm/min found here).

As illustrated in Figures 2 and 3, the penetration rates into quenched films clearly exceed those into annealed films; i.e., they exhibit the same tendency previously observed by CD[4] (cf. Figure 18 therein), although the magnitude of the effect here is much smaller. The reason for the much more pronounced effect of quenching noted by CD (which also greatly exceeds that found by Windle[10] in penetration across free films) is most probably to be sought in the inability

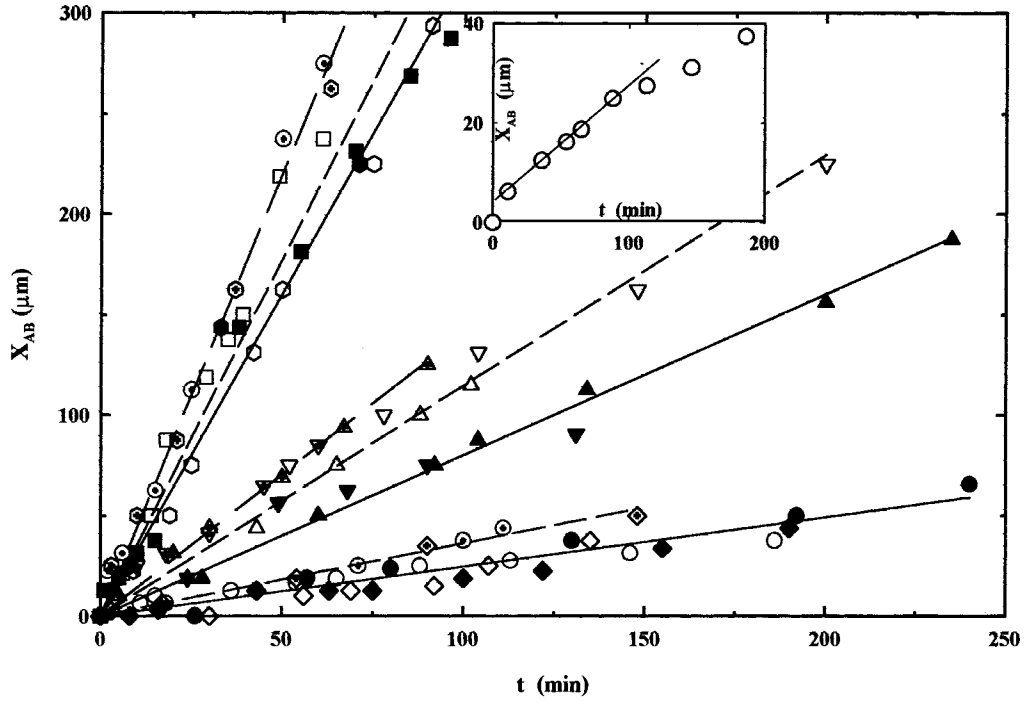

Figure 2. Kinetics of penetration into sandwiched film at 22 (circles, diamonds), 30 (triangles), or 40 °C (squares, hexagons). The free film ($L = 30-40$ μm) had previously been annealed (filled points), quenched in ice water (open points), or quenched in liquid N_2 (open points with dots).

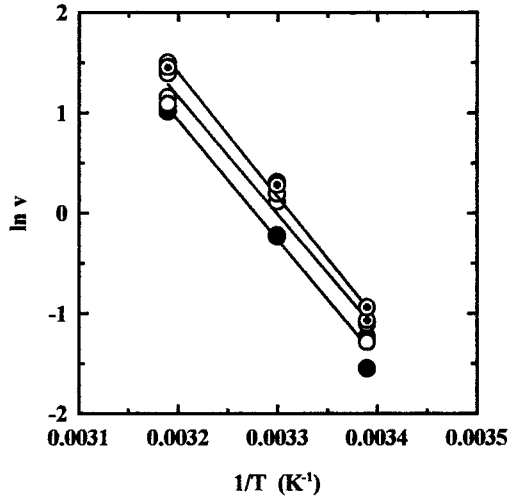

Figure 3. Arrhenius plots of penetration velocities into sandwiched film which had previously been annealed (filled points), quenched in ice water (open points), or quenched in liquid N_2 (open points with dots).

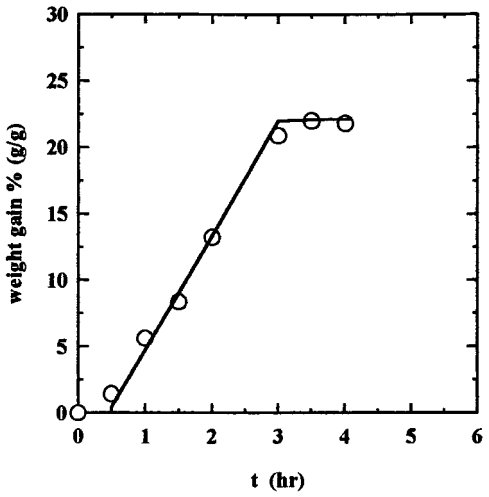

Figure 4. Measured fractional weight gain of free film (points) at 22 °C compared with a line of slope calculated from the corresponding rate of penetration into sandwiched film.

of the film to retract upon quenching, due to adhesion to the support. Similarly, the magnitude of the effect was found by CD[4] and Windle[10] to increase with the severity of the treatment (notably the rate of cooling), and the same result was obtained here by quenching the free film in ice water or liquid N_2 (cf. Figure 2). As shown in Figure 3, the Arrhenius plot of penetration rate tends to deviate from linearity rather more in quenched than in annealed film, but no clear trend of the overall value of E_v^a (=23.3 ± 0.9 and 24.5 ± 0.6 kcal/mol for film quenched in ice water and liquid N_2 respectively) between 22 and 40 °C, as a result of quenching, can be established with any certainty. The corresponding data reported by CD[4] are also rather limited in this respect.

Penetration Profiles. Typical examples of observed fringe patterns are given in Figure 5 and typical normalized OPD profiles deduced therefrom, over the temperature range studied, for annealed and quenched films, are shown (at a standard distance of penetration $X_{AB} = 40$ μm) in Figures 6 and 7, respectively.

As indicated in the Experimental Section, the normalized OPD profile may be expected to reproduce faithfully the corresponding (suitably normalized) concentration profile, under conditions of uniform specimen thickness and linear dependence of refractive index on concentration. As discussed in previous papers,[8,9] glassy polymer−penetrant systems usually deviate, to a greater or lesser extent, from the latter condition at lower concentrations, mainly as a result of the presence of excess free volume. Marked deviations of the kind reported in refs 8 and 9 are certainly absent here,

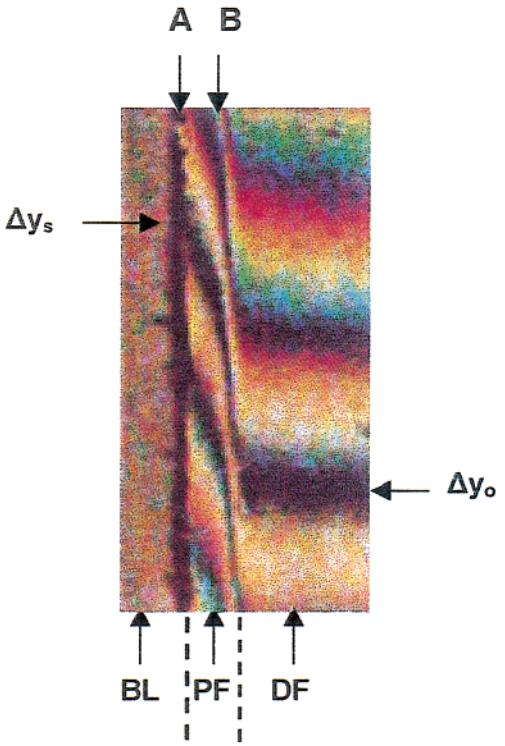

Figure 5. Photograph of typical interference fringe pattern characteristic of penetrated sandwiched film. Annealed film ($L = 34\ \mu$m) at 22 °C. BL = bulk liquid MA; PF = penetrated film; DF = dry film; A = front A ($x = 0$); B = front B ($x = X_{AB}$); Δy_s = OPD at $x = 0$; Δy_o = OPD of dry film. The fringes in the bulk MA are outside the optical field covered by this photograph.

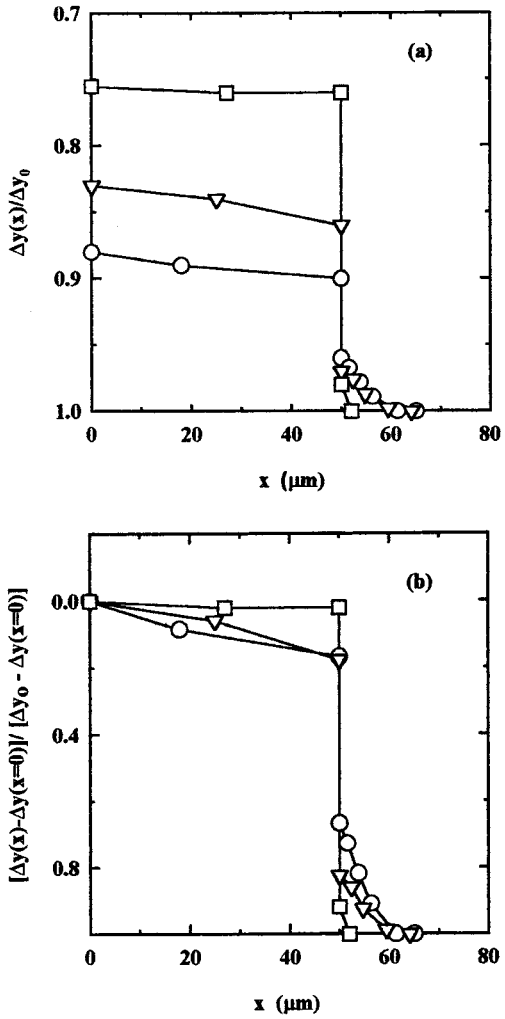

Figure 6. (a) Optical path difference (OPD) profiles in penetrated sandwiched annealed films, normalized with respect to the OPD of unpenetrated film and plotted so as to reflect the corresponding normalized concentration profile (see eq 2a) and (b) OPD profiles as above but normalized to the same surface OPD, at 22 (○), 30 (▽), or 40 °C (□); L (μm) = 33 (○), 33 (▽), and 31 (□).

although some distortion of the low concentration profile emanating from this source is not, of course, excluded.

On the other hand, the uniform thickness condition may, in principle, always be imposed by the application of clamping pressure sufficiently high to suppress significant swelling in the direction of the film thickness. However, such extreme, externally imposed restriction of swelling is undesirable, because it entails marked modification of the transport phenomena under study.[9] Fortunately, such problems do not arise if the penetrant is a strong plasticizer of the polymer, as is the case here (DSC measurements on the swollen film at a heating rate of 10 °C/min showed drops of T_g amounting to 95−105 °C for polymer weight fractions of 0.69−0.75). Under such conditions, restriction of thickness dilation is confined to a narrow low concentration region, because the polymer is soon plasticized to the point where it can relax by yielding under the moderate clamping pressure applied by the spring clips. From that point on, the deficiency in thickness dilation can be made up (or nearly so) by additional (plastic) dilation in the $-x$ direction, with the result that uniformity of specimen thickness is not significantly disturbed.[9] This transport mechanism is not basically different from that seen in penetration into a free film.[11] In the latter case, the x axis is directed along the film thickness, while dilation along the plane of the film tends to be suppressed (by the *internal* constraint imposed by the rigid unswollen core of the film,[12,13] which was not included in the preceding discussion for the sake of simplicity) and reappears as additional dilation in the $-x$ direction.[14] A difference between penetration into free and sandwiched films, which may be worth noting, is that dilation in the $-x$ direction is perfectly free in the former case but is subject to some frictional resistance (minimized by suitable lubrication of the confining glass plates; see Experimental Section and ref 9) in the latter case, which may also contribute noticeably to restriction of swelling in the low concentration region.

On the basis of the foregoing discussion, it appears that the OPD profiles presented above may be expected to represent realistically the concentration profiles of interest here but should not be relied on to reproduce faithfully the finer details of the shape of the low concentration (precursor) profile or of the sharp front.

Annealed Films. The data presented in Figure 6 exhibit all the general characteristics of case II diffusion profiles: namely a sharp front, a flat high concentration profile behind the sharp front, and a diffuse low-concentration profile ahead of the sharp front. The last-mentioned feature confirms the results of CD's interferometric technique, as opposed to those of TW's microdensitometric technique. The inability of the latter experimental method to detect even substantial precursor fronts, was demonstrated by the performance of experiments at 22 °C with added iodine tracer, as

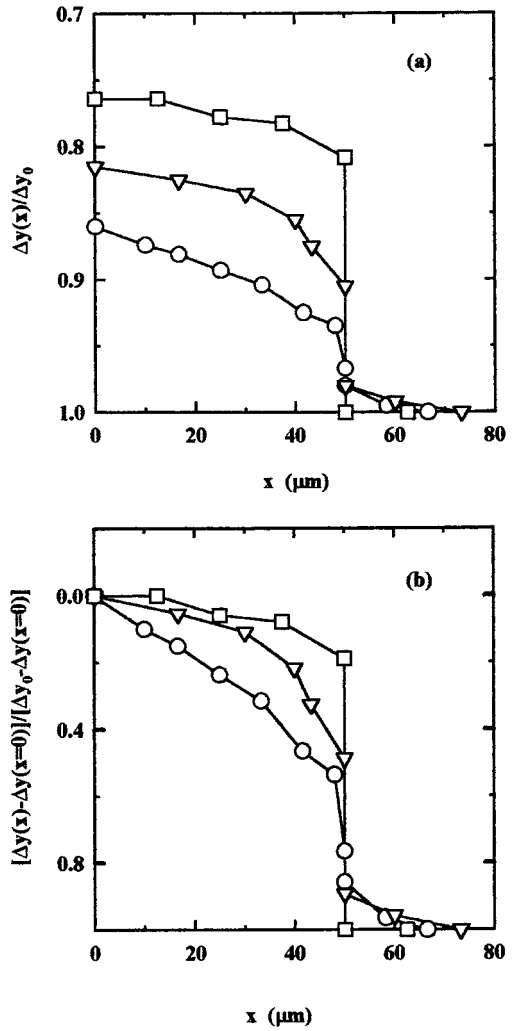

Figure 7. OPD profiles as in Figure 6, but for films quenched in ice water. Notation as in Figure 6: L (μm) = 31 (○), 30 (▽), and 33(□).

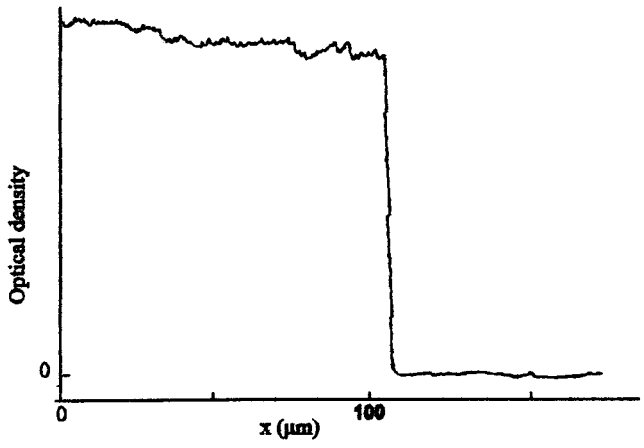

Figure 8. Iodine tracer optical density profile in sandwiched annealed film penetrated by MA at 22 °C.

described in the Experimental Section. A typical experimental iodine optical density profile is displayed in Figure 8.

As shown in Figure 6, increase in temperature, in the range 22−40 °C, is accompanied (1) by rising solubility of liquid methanol in the polymer, in agreement with previous results,[2,4] and (2) by sharpening of the overall penetration front, in agreement with the rising reflectivity of the said front observed by CD (see Figure 15 in ref 4).

The present data show further that the above change in profile shape is attributable to (a) shrinking of the precursor front and (b) more pronounced flattening of the high concentration profile. The former effect, which is the primary one, provides direct experimental confirmation of the mechanism proposed by CD[4] for the increase in reflectivity of the penetration front. In particular, the correlation[1,3,6,7] $v_o \sim \sqrt{\beta_o D_o}$, in conjunction with the observation that the temperature dependence of v_o ($E_v^a \cong 24$ kcal/mol) is much steeper than that of D_o ($E_D^a \cong 15$ kcal/mol),[15] means that $\tilde{\beta}_o = \beta_o X_{AB}^2/D_o$ (defined in part 1 and reformulated here in a manner appropriate for the situation under consideration) rises with temperature. This, in turn, implies shrinkage of the precursor front (which has been put in evidence more clearly, by removing the effect of temperature on MA solubility, in Figure 6b). Effect b, on the other hand, implies that $D_F/\beta_o X_{AB}^2$ tends to increase with temperature and the corresponding rise of MA solubility (cf. relation 14b and Figure 3 in part 1). The fact that E_D^a is enhanced upon passage to the rubbery state, in conjunction with the observation that $T_g \cong T$ in the swollen polymer region at $T = 22$ °C, means that the temperature dependence of D_F will be enhanced at higher T and thus helps to explain why effect b is considerably more marked between 30 and 40 °C than between 22 and 30 °C. On the other hand, this effect should be of smaller significance in CD's data,[4] in view of the considerably lower penetration distances X_{AB} involved.

The present results also provide material experimental evidence with respect to the observation that the rise of front reflectivity with temperature, shown in Figure 15 of ref 4, attains a maximum at $T \cong 45$ °C and changes to a decline thereafter. This occurs although the rise of v_o at higher T continues unabated (cf. Figures 11 and 12 of ref 4). As pointed out by CD,[4] this behavior runs counter to the theoretical expectation based on effect a, which requires the precursor front to keep shrinking, as long as $\tilde{\beta}_o$ continues to increase with rising temperature.

A way out of this theoretical impasse is provided by the demonstration in Figure 6 that the precursor front is barely detectable at 40 °C and hence must be very near the vanishing point at $T \cong 45$ °C. It follows that effect a actually runs its full theoretically prescribed course (which simply terminates at the reflectivity maximum) and that another effect (possibly preexisting but masked by effect a) must be invoked to explain the reflectivity behavior observed beyond this point.

From the mathematical point of view, and within the bounds of the modeling work of part 1, two such possibilities could be put forward. One is reversal of effect (b) at $T > 45$ °C, implying reversal of the aforementioned trend at $T \leq 40$ °C of the parameter $D_F/\beta_o X_{AB}^2$. The other possibility is decline of the steepness of the sharp front, due to diminution of β_F/β_o (which, incidentally, also entails reappearance of the precursor profile; see Figure 5 of part 1). On the basis of eq 21a of part 1, such an effect, which may be termed effect c, is to be expected only if the rise of β_F/k_B at $T \geq 45$ °C is superseded by that of v_o.

Quenched Films. The present experimental results also yield crucial evidence concerning the effect of

quenching and the difficulty encountered by CD[4] in formulating a consistent interpretation of the resulting observed behavior of penetration front reflectivity. In particular the said reflectivity was found to increase with rising temperature in the range $T < 45$ °C, in line with what was seen in annealed films and hence in keeping with effect a (see above). On the other hand, the reflectivity values recorded were found to be much lower for quenched than for annealed films. As shown by CD,[4] interpretation of this result, in terms of a more pronounced precursor profile in quenched films, runs counter to the observation that penetration rate is enhanced by quenching (as noted above), *not* reduced as would be expected theoretically on the basis of effect a.

The data of Figure 7 confirm those of CD[4] in that (i) the solubility of liquid MA is not substantially different from that in annealed films (cf. Figure 9) and (ii) the overall penetration front becomes steeper with rising temperature, while (iii) the said front is less steep in quenched, than in annealed, films (cf. Figure 9).

However, our data also bring out the crucial new point that feature iii is clearly attributable to a reverse effect b (i.e. steepening of the flat profile behind the sharp front), which (as explained in part 1) is perforce combined with effect c (loss of steepness of the sharp front). The latter effect becomes prominent enough to be easily visible at 22 °C. Interestingly, there is a discernible general tendency for the precursor front to shrink upon quenching, so the theoretical expectation in terms of effect a mentioned above is *not* contradicted: effect a is simply overwhelmed by the other more prominent ones.

As noted above, steepening of the flat profile behind the sharp front implies lowering of $D_F/\beta_0 X_{AB}^2$, which is eventually reflected in significant deviation from case II kinetics (due to partial diffusion control of the penetration rate). Such a deviation is, indeed, discernible in the penetration data for a quenched film at 22 °C (illustrated more clearly in the inset of Figure 2). This result is in line with more detailed observations of penetration across films precooled at different rates through T_g, which show increasing deviation from case II kinetics with increasing precooling rate (see Figure 4 of ref 16). The relevant measurements extend over larger penetration distances than those of the present work, which, in turn, considerably exceed those of CD.[4] Hence, the value of $D_F/\beta_0 X_{AB}^2$ would be expected to be correspondingly higher in ref 4, but this must be weighed against the fact that the effect of quenching (as gauged by the magnitude of the induced change in v_0) is much more pronounced in ref 4.

Thus, interpretation of the effect of quenching on front reflectivity seen by CD,[4] in terms of steepening of the flat profile and/or loss of steepness of the sharp front, seems quite plausible. A physical basis for this interpretation is provided by the well-known fact that quenching raises the T_g of the polymer (a rise of the order of 3 °C, just within the capability of our DSC instrument, was indicated in the present case). This may be expected to have a dual effect on the parameters $D_F/\beta_0 X_{AB}^2$ and β_F/β_0 (which largely control the features of the penetration profile considered above, see part 1) for quenched, as compared with annealed, films. On one hand, β_0 should be enhanced thanks to the increase in free volume associated with higher T_g. On the other hand, D_F and β_F will tend to be lower, when the swollen polymer is in the transition region, because quenched films will tend to be more "glassy" than annealed ones. This lowering of D_F and β_F may be expected to be substantial at 22 °C (where $T \cong T_g$ of the swollen polymer, as previously mentioned) and to diminish with rising temperature, thus yielding a steeper increase in D_F with temperature in quenched, than in annealed, films, thus accounting for the strong effect b shown in Figure 7.

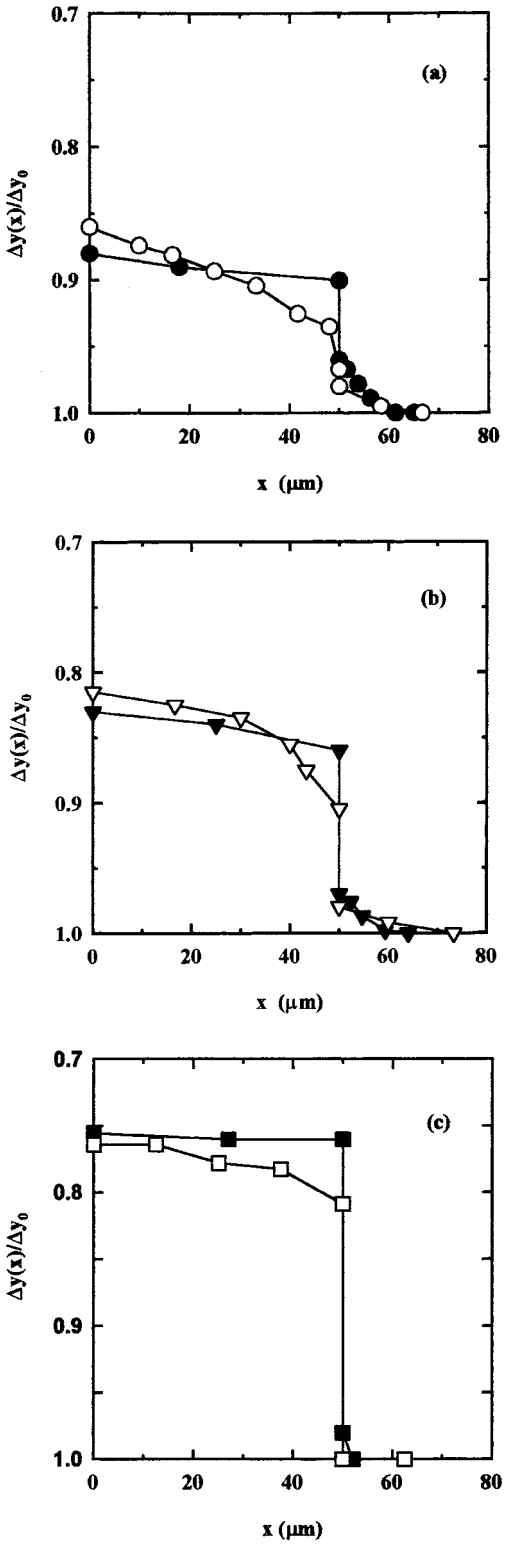

Figure 9. Detailed comparison of the annealed (filled points) and quenched (open points) film profiles presented in Figures 6 and 7: (a) 22 °C; (b) 30 °C; (c) 40 °C.

On the other hand, as also shown in Figure 7, effect a runs, here too, its full theoretically prescribed course (which terminates at $T \cong 40$ °C).

Summary and Conclusions

The results presented and discussed in the preceding section fully confirm our original expectation that the experimental approach adopted here can provide substantial further insight into important aspects of case II transport behavior in the PMMA−MA system previously studied by TW[2,3] and CD.[4,5] This approach has the advantage of yielding a direct, in situ picture of the penetrant distribution profile, not subject to reliance on a colored tracer[2,3] or on a model-dependent interpretation of an interference pattern.[4]

With regard to the TW technique,[2,3] it has been shown beyond doubt that the iodine tracer used therein cannot show up the presence of the diffuse precursor front.

On the other hand, the complementarity of the interferometric technique used in CD's work[4] with the present one is noteworthy. It is mainly due to the high sensitivity of the former technique to changes in steepness of the sharp front. Thus, combination of the present experimental results with those of CD, in the light of a more sophisticated model approach (made possible by the work reported in part 1), has led to much clearer understanding of the phenomena under study. In this respect, it was quite fortunate that the annealed films studied here exhibited MA sorption and transport properties closely resembling those of the corresponding films of CD. Sorption properties were little affected by quenching in both cases. The effect of quenching on penetration rate was also similar, even though it was quantitatively much more pronounced in CD's data[4] (a difference attributable to the fact that the quenching treatment was applied to free films here and to supported films in CD's work).[4]

More specifically, the present results (i) demonstrate that increase of penetration velocity with rising temperature, below 45 °C, is accompanied by shrinkage of the precursor profile, in line with what is predicted theoretically,[1,3,4,7] when $\tilde{\beta}_o = \beta_o X_{AB}^2/D_o$ is an increasing function of temperature, thus confirming CD's interpretation[4] of the corresponding observed sharpening of the overall penetration front; (ii) throw light on the question (left open in CD's work)[4] as to why the aforesaid sharpening does not continue (in line with the above interpretation) but is reversed at $T > 45$ °C, by showing that the precursor front shrinks to the vanishing point at $T \cong 45$ °C and another mechanism (probably involving the steepness of the sharp front itself) appears to come to the fore; (iii) help to resolve the question (left open in CD's work)[4] as to why the increase in penetration velocity induced by quenching is accompanied by (marked) loss of sharpness of the overall penetration front, instead of an expected gain reflecting (see point i above) shrinkage of the precursor front. The answer to the question posed in point iii above is that significant shrinkage of the precursor front does, indeed, occur but is overshadowed by a pronounced loss in steepness of the sharp front.

Acknowledgment. This work was partially supported by internal Grant No. 602 in the framework of the "Demoerevna" Program of the National Research Center Demokritos.

References and Notes

(1) Part 1: Sanopoulou, M.; Stamatialis, D. F.; Petropoulos, J. H. *Macromolecules* **2001**, *34*, 1012.
(2) Thomas, N.; Windle, A. H. *Polymer* **1978**, *19*, 255.
(3) Thomas, N. L.; Windle, A. H. *Polymer* **1982**, *23*, 529.
(4) Durning, C. J.; Hassan, M. M.; Tong, H. M.; Lee, K. W. *Macromolecules* **1995**, *28*, 4234.
(5) Hassan, M. M.; Durning, C. J. *J. Polym. Sci., Part B: Polym. Phys. Ed.* **1999**, *37*, 3159.
(6) Hui, C. Y.; Wu, K. C.; Lasky, R. C.; Kramer, E. J. *J. Appl. Phys.* **1987**, *61*, 5129.
(7) Hui, C. Y.; Wu, K. C.; Lasky, R. C.; Kramer, E. J. *J. Appl. Phys.* **1987**, *61*, 5137.
(8) Sanopoulou M.; Petropoulos, J. H. *J. Polym. Sci., Part B: Polym. Phys. Ed.* **1992**, *30*, 983.
(9) Stamatialis, D. F.; Sanopoulou, M.; Petropoulos, J. H. *J. Appl. Polym. Sci.* **1997**, *65*, 317.
(10) Windle, A. H. *J. Membr. Sci.* **1984**, *18*, 87.
(11) Petropoulos, J. H. *J. Polym. Sci., Part B: Polym. Phys. Ed.* **1984**, *22*, 183.
(12) Petropoulos, J. H.; Roussis, P. P. *J. Membr. Sci.* **1978**, *3*, 343.
(13) Gostoli, C.; Sarti, G. C. *Polym. Eng. Sci.* **1982**, *22*, 1015.
(14) Thomas, N.; Windle, A. H. *J. Membr. Sci.* **1978**, *8*, 317.
(15) Arnould, D.; Laurence, R. L. In *Inverse Gas Chromatography: Characterization of Polymers and Other Materials*; ACS Symposium Series 391; American Chemical Society: Washington, DC, 1989; p 87.
(16) Thomas, N.; Windle, A. H. *Polymer* **1980**, *21*, 613.

MA001409B